Materials Science-Poland, 34(1), 2016, pp. 148-156
http://www.materialsscience.pwr.wroc.pl/
DOI: 10.1515/msp-2016-0017

DE GRUYTER OPEN

Fabrication and characterization of nanostructured Ba-doped $BiFeO_3$ porous ceramics

E. MOSTAFAVI, A. ATAIE*

School of Metallurgy and Materials Engineering, College of Engineering, University of Tehran,
P.O. Box 14395-553, Tehran, Iran

Nanostructured barium doped bismuth ferrite, $Bi_{0.8}Ba_{0.2}FeO_3$ porous ceramics with a relatively high magnetic coercivity was fabricated via sacrificial pore former method. X-ray diffraction results showed that 20 wt.% Ba doping induces a structural phase transition from rhombohedral to distorted pseudo-cubic structure in the final porous samples. Moreover, utilizing $Bi_{0.8}Ba_{0.2}FeO_3$ as the starting powder reduces the destructive interactions between the matrix phase and pore former, leading to an increase in stability of bismuth ferrite phase in the final porous ceramics. Urea-derived $Bi_{0.8}Ba_{0.2}FeO_3$ porous ceramic exhibits density of 4.74 g/cm^3 and porosity of 45 % owing the uniform distribution of interconnected pores with a mean pore size of 7.5 μm. Well defined nanostructured cell walls with a mean grain size of 90 nm were observed in the above sample, which is in a good accordance with the grain size obtained from BET measurements. Saturation magnetization decreased from 2.31 in the $Bi_{0.8}Ba_{0.2}FeO_3$ compact sample to 1.85 A·m^2/kg in urea-derived $Bi_{0.8}Ba_{0.2}FeO_3$ porous sample; moreover, coercivity increased from 284 to 380 kA/m.

Keywords: *bismuth ferrite; dopant; nanostructures; porous ceramics; magnetic properties*

1. Introduction

Porous magnetic materials are an expanding field of study in multifunctional applications [1]. Also, the correlation between porosity with magnetic and ferroelectric properties has received a great deal of attention in the recent years. Coexistence of ferromagnetic and ferroelectric properties in the multiferroic materials provides potential applications in the magnetic-field sensors and detectors, memory devices, spintronics, photovoltaics, optical filters and magnetic-recording media [2–4]. Combination of promising applications of multiferroic materials with unique properties of porous ceramics, such as high surface area, high strength and high chemical resistivity, could open up a new field of study in advanced materials [5].

Bismuth ferrite, $BiFeO_3$ (BFO), is perhaps the only multiferroic material with a coexistence of ferroelectric and magnetic ordering at room temperature [6]. $BiFeO_3$ possesses a rhombohedrally distorted perovskite structure with R3c space group, high ferroelectric Curie temperature ($T_C \sim 830$ °C) and G-type antiferromagnetic Neel temperature ($T_N \sim 370$ °C). Since $BiFeO_3$ is very sensitive to the synthesis conditions, and a small deviation from the stoichiometric ratio can lead to the formation of impurity phases such as $Bi_2Fe_4O_9$ and $Bi_{25}FeO_{40}$ [7–9], synthesis of the single-phase $BiFeO_3$ by conventional solid state reaction method remains challenging. Khomchenko et al. [10] have reported that doping Bi site of $BiFeO_3$ by diamagnetic ions with bigger ionic radius can be a promising way for achieving the single-phase bismuth ferrite with better multiferroic properties. On the other hand, the density of bismuth ferrite (8.4 g/cm^3) is significantly higher than that of other ferrites [11, 12]. Therefore, the ability to reduce its bulk density, while preserving the single-phase pervoskite structure and its multifunctional properties, is of a great importance. Particularly, developing a combination of multiferrioc and porous ceramics is desired.

*E-mail: aataie@ut.ac.ir

Porous ceramics have a variety of applications in filters, water purification, sorbents, catalysis, biomedical devices, gas separation membranes, chemical sensors, lightweight structural materials, components in the batteries, and solid oxide fuel cells (SOFCs) [13–15]. There are several processing routes for fabrication of porous ceramics [15]. Three of them were systematically illustrated by Studart et al. [14] as replica, sacrificial pore former and direct foaming techniques. Among these methods "Sacrificial Pore Former Method" (SPFM) is a relatively simple technique and has some advantages in comparison with the other fabrication methods. For instance, porosity, pore size distribution, and pore morphology of the final porous components can be controlled through the appropriate choice of the sacrificial materials. There are some reports emphasizing that undesired reactions could happen between the matrix phase and pore former at elevated temperatures [13–16]. Xiao et al. [17] reported that urea can be an appropriate pore forming agent to fabricate polymer electrolyte membrane for lithium-ion battery. Hong-Tao et al. [18] fabricated porous Co–Fe spinel using 0 to 50 wt.% graphite as the pore former. They found that with adding graphite up to 20 wt.% the porosity increases rapidly. Also, graphite powder has only slight influence on decomposition of the matrix material, and its pore forming effects are quite favorable.

Microporous ceramics with nanosized grains on the cell walls have attracted attention because of their unique and astonishing properties, such as high specific surface area. Nanostructured bismuth ferrite shows strong size-dependent magnetic properties [19] and has been studied for the potential use as a gas sensor for sensing ethanol and acetone [20]. Previously, an attempt was made to achieve appropriate conditions for synthesizing the single-phase bismuth ferrite by substitution of Ba^{2+} into Bi^{3+} sites [21]. Previous studies revealed that among all Ba-doped $BiFeO_3$ compounds, $Bi_{0.8}Ba_{0.2}FeO_3$ exhibits maximum magneto-electric coupling, better fatigue resistance, best ferroelectric hysteresis loop, enhanced multiferroic properties as well as the highest activation energy which leads to better performance as dielectric material [21–24].

To the best of our knowledge, the fabrication of single-phase porous bismuth ferrite ceramics has not been reported. In the present study, we report on the fabrication of single-phase nanostructured bismuth ferrite porous ceramics with a relatively high magnetic coercivity via sacrificial pore former method. Particularly, the effects of dopant on the phase evolution of the final porous samples, the physical and microstructural changes caused by applying various pore formers as well as the influence of porosity on the magnetic properties of porous bismuth ferrites have been investigated.

2. Experimental

Nanostructured $Bi_{0.8}Ba_{0.2}FeO_3$ (BBFO) powder was synthesized by the conventional solid-state reaction method using high purity analytical grade Bi_2O_3, Fe_2O_3 and $BaCO_3$ (purity $\geqslant$ 99 %) reagents. The fabrication of porous bismuth ferrite ceramics was carried out by sacrificial pore former method (SPFM). Ba-doped bismuth ferrite powder was mixed with 30 wt.% of various pore formers (high density polyethylene (HDPE), polyvinyl alcohol (PVA), urea and graphite) and then ball milled for 10 h in a high energy planetary ball mill. Ball to powder mass ratio (BPR) and rotation speed were 20 and 300 rpm, respectively. Table 1 lists the description of different porous samples and specifications of PFs used in this study.

The obtained uniform powders mixtures were uniaxially cold pressed at a constant applied pressure of 50 MPa to form pellets with a 12.6 mm diameter. Then, these pellets were sintered at 870 °C for 1 h in an air atmosphere under a multi-step regime, as presented schematically in Fig. 1. In this regime, low heating rate of 1 °C/min was chosen up to 400 °C, for the complete burnout of the sacrificial material in bismuth ferrite matrix before the sintering started. The dwell time was set to 1 h at temperatures of 150, 250 and 400 °C, in order to avoid destruction of residual matrix structure [14]. The reasons behind the selection of sintering temperature of 870 °C for 1 h is explained

Table 1. Porous samples code and specification of sacrificial pore former materials.

Sample code	Porous sample identity (Matrix/wt.% of PFs)	Sacrificial pore Formers specification			
		Density [g/cm^3]	Melting point [°C]	Purity [%]	Resource
BBH	BBFO/30HDPE	0.95	130	Commercial	–
BBP	BBFO/30PVA	1.26	230	>99.0	Merck
BBU	BBFO/30Urea	1.32	133 – 135	>95.0	Merck
BBG	BBFO/30Graphite	2.16	–	>99.0	MP Biomedicals
BBC	BBFO-Compact	–	–	–	–

elsewhere [25]. A compact sample of BBFO starting powder (without pore former) was also processed and sintered under the identical conditions, denoted as BBC sample.

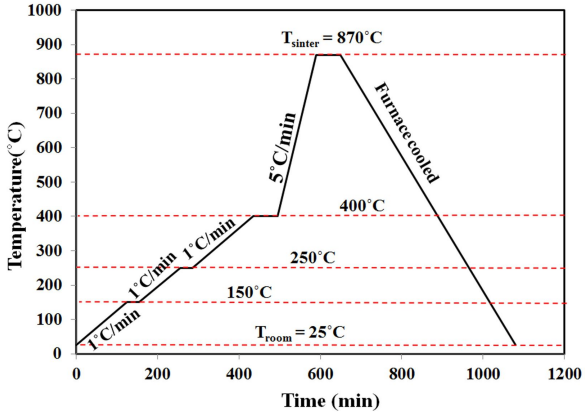

Fig. 1. Multi-step heat treatment cycle of samples sintered at 870 °C for 1h.

The phase characterizations of the samples was performed by X-ray diffraction (XRD) at room temperature utilizing Philips PW-1730 with CuKα radiation ($\lambda = 1.5406$ Å) in the range of $20° \leqslant 2\theta \leqslant 70°$ and step size of 0.02°. The mean crystallite size of the samples was calculated using Scherrer formula [26].

The microstructure of the samples was studied by field emission scanning electron microscope (FESEM, Hitachi S4160). The mean grain size of nanostructured cell walls of the porous samples was measured by two different methods: (1) utilizing FESEM micrographs and standard image analyzer MIP (Microstructure Image Processing) software, and (2) by employing specific surface area (S_{BET}) obtained from nitrogen adsorption. Specific surface area of the porous BBU sample was determined by nitrogen adsorption using Brunauer, Emmet, and Teller (BET) isotherm. Density and relative porosity of the sintered samples were measured by Archimedes water immersion method with a theoretical density of 8.4 g/cm^3 for the bulk bismuth ferrite. Magnetic properties of the specimens were measured by vibrating sample magnetometer (VSM) at room temperature under the maximum applied magnetic field of 1200 kA/m.

3. Results and discussion

Fig. 2 shows the XRD patterns of BBFO/PFs samples after sintering at 870 °C for 1 h. Analysis of the XRD patterns confirmed the single-phase bismuth ferrite for BBU and BBC samples. A partial decomposition of $Bi_{0.8}Ba_{0.2}FeO_3$ phase was observed in the BBH, BBP and BBG samples due to the intensive reactions between thermal decomposition products of pore formers and bismuth ferrite matrix phase at elevated temperatures.

It is clearly evident from Fig. 3 that by 20 wt.% Ba doping, all the double or triple peaks merge together in the final porous ceramics, which could be due to a structural phase transition from distorted rhombohedral to pseudo-cubic structure [21]. However, XRD results revealed that by employing $Bi_{0.8}Ba_{0.2}FeO_3$ as the starting powder, the phase composition of final porous samples was greatly improved, as presented in Fig. 3. This phenomenon was also observed for the other samples. It seems Ba-dopant has an inhibiting effect on the formation of secondary phases such as $Bi_2Fe_4O_9$ and $Bi_{25}FeO_{40}$. Moreover, Ba^{2+} ions can dramatically suppress the tendency of reactions

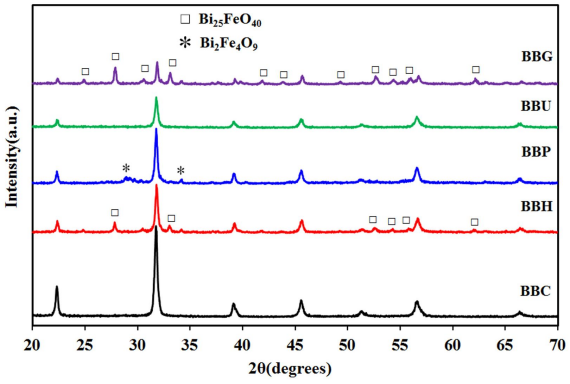

Fig. 2. X-ray diffraction patterns of BBFO/PFs porous samples after sintering at 870 °C, 1 h.

between the thermal decomposition products of pore formers and the matrix phase at elevated temperatures. Additionally, it can suppress the kinetics of the decomposition reaction of bismuth ferrite according to the following reaction [8, 27]:

$$49BiFeO_3 = 12Bi_2Fe_4O_9 + Bi_{25}FeO_{40} \quad (1)$$

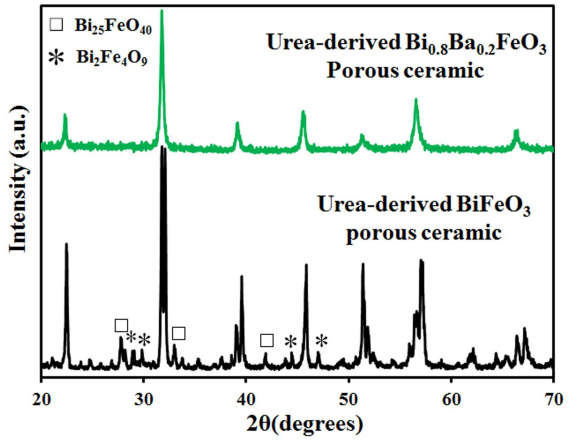

Fig. 3. X-ray diffraction patterns of urea-derived $BiFeO_3$ and $Bi_{0.8}Ba_{0.2}FeO_3$ porous ceramics sintered at 870 °C, 1 h.

Since Ba ions have a larger ionic radius (R_{Ba}^{2+} = 1.42 Å) compared to that of Bi ions (R_{Bi}^{3+} = 1.17 Å), thus by substitution of 20 wt.% Ba^{2+} ions instead of Bi^{3+} ions the Goldschmidt's tolerance factor (t) increases. It is well known that the structural stability of perovskite compounds can be quantified by this factor. Here, we obtained t = 0.886 and 0.904 for BFO and BBFO compounds, respectively using the effective ionic radius of Shannon [28]. Moreover, Selbach et al. [8] showed that substitution of Bi^{3+} with a larger cation could increase the stability of $BiFeO_3$ phase with respect to the secondary phases of mullite ($Bi_2Fe_4O_9$) and sillenite ($Bi_{25}FeO_{40}$). Therefore, in the present study, with enhancing the stability of the starting perovskite powder, the thermal decomposition products of PFs were not able to easily influence the final structure. In contrast, in the absence of Ba^{2+} ions, $BiFeO_3$ matrix phase has been dramatically destructed [25]. It is worth noting that the impurity phases of BBG and BBH samples are bismuth-rich phases of $Bi_{25}FeO_{40}$. Contrary to this, for BBP sample, the major impurity phase is bismuth-deficient phase ($Bi_2Fe_4O_9$). The reason for this anomaly is not very clear at present. Generally, bismuth rich compounds are naturally volatile ($Tm_{(Bi)}$ = 271.4 °C, $Tm_{(Bi2O3)}$ = 825 °C and $Tm_{(Bi25FeO40)}$ = 785 °C), thus the evaporation of these compounds during heat treatment may result in degradation of the $BiFeO_3$ phase. Hence, the partial substitution of Bi^{3+} by Ba^{2+} can suppress the evaporation of bismuth site and lead to the stability enhancement of $BiFeO_3$ phase [21, 29].

Density and relative porosity of BBFO/PFs porous samples are shown in Fig. 4. It should be noted that the maximum applicable amount of the sacrificial pore former varied with the type of the pore former. However, 30 wt.% was selected as an appropriate constant amount for micro-structure comparison. For instance, applying 30 wt.% of HDPE pore former resulted in collapsed structure, but this sample was valuable for further experiments. As seen in Fig. 4, the highest porosity among BBFO/PFs samples was observed in the BBG sample. This might be related to the exothermic reactions between graphite and oxygen which is associated with enhanced CO and CO_2 exhaust gases, and leads to an increase in the porosity [30]. Furthermore, the discrepancies in relative porosity of BBFO/PFs samples could be interpreted as the different pore morphologies which depend on the type of PFs. It is well known that the volume

shrinkage of spherical pores is the least among all the various shapes of the pores when it is subjected to the same shrinkage [31]. The pores obtained from BBP and BBG samples are almost spherical (Fig. 5), while the pores of the BBU sample have been formed with irregular shapes. Hence, for the same weight fraction of the pore formers, relative porosity of those containing spherical pores is at the highest level. Therefore, one can relate these small discrepancies to the different characteristics of the pore formers. However, it is noteworthy that increasing of porosity is not the only way for selecting an appropriate pore former as well as more applicable porous samples [32].

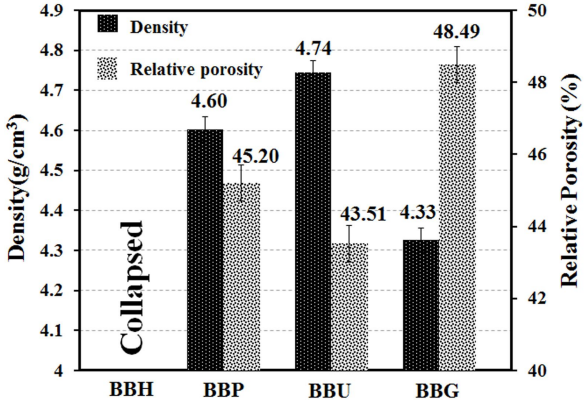

Fig. 4. Density and relative porosity of BBFO/30PFs porous samples.

It is noticeable that utilizing $Bi_{0.8}Ba_{0.2}FeO_3$ as a starting powder enhances the mechanical strength of the final porous sample. This could be related to the higher stability as well as better sinterability of the bismuth ferrite structure in the presence of 20 wt.% Ba^{2+} instead of Bi^{3+} ions [21].

Fig. 5 shows the microstructures of BBFO/PFs samples. Isolated closed pores with spherical shapes within the microstructures were observed for BBP and BBG samples (Fig. 5b and 5d), while in the BBU sample irregular interconnected pores were formed (Fig. 5c). Indeed, the pore morphology and porosity of porous samples were affected by altering pore forming agents. For instance, spherical pores of BBP sample compared to irregular shape pores of BBU sample could be interpreted by the various behaviors of the pore formers during the cold pressing and subsequent heat treatment.

Fig. 6 demonstrates the microstructure of the BBU sample at low and high magnifications. Uniform distribution of pores with the mean pore size of 7.5 μm was measured for BBU sample (Fig. 6a). It was reported that using urea as a pore former gives porous ceramics with a mean pore diameter of 7 μm, uniform pore distribution as well as open pores, which confirmed the accuracy of the obtained results in the present study [25]. Also, Fig. 6b shows that in the BBU porous sample, nanostructured cell walls with obviously interconnected pores and well-developed necking appear between the bismuth ferrite grains. The mean grain size on the pore walls of the above sample was 90 nm. Such a uniform distribution of interconnected pores, together with the multi-functional lightweight porous structure ($\rho_{BBU\,porous} = 4.74$ g/cm^3 compared to bulk BFO with 8.4 g/cm^3) can be a suitable candidate for various applications [17, 32]. In addition, by comparing FESEM images of BBFO powder as the starting matrix material with the grains on the cell walls of the BBU sample, it is realized that the grain growth is negligible during sintering at 870 °C for 1 h [21].

Fig. 7 shows the magnified FESEM images of BBP and BBG samples. It is clearly seen that some hexagonal shaped grains were formed in these samples. As indicated in Fig. 7b of BBG sample, in some regions there are hexagonal grains with the mean thickness of 500 nm and the width of 5 μm, tangled with each other and forming a three-dimensional pores network. It is noticeable that due to the substitution of Ba^{2+} into $BiFeO_3$ structure, the Goldschmidt's tolerance factor (t) increased, and then, the hexagonal variants of the perovskite structure were stable [33]. Moreover, this morphological transformation could be interpreted by the presence of Ba^{2+} and PFs beside $BiFeO_3$ phase. This might have influenced the rate of nucleation and growth, and subsequently led to increasing particle growth rate along another direction which is obviously different from primary direction of <1 1 0>.

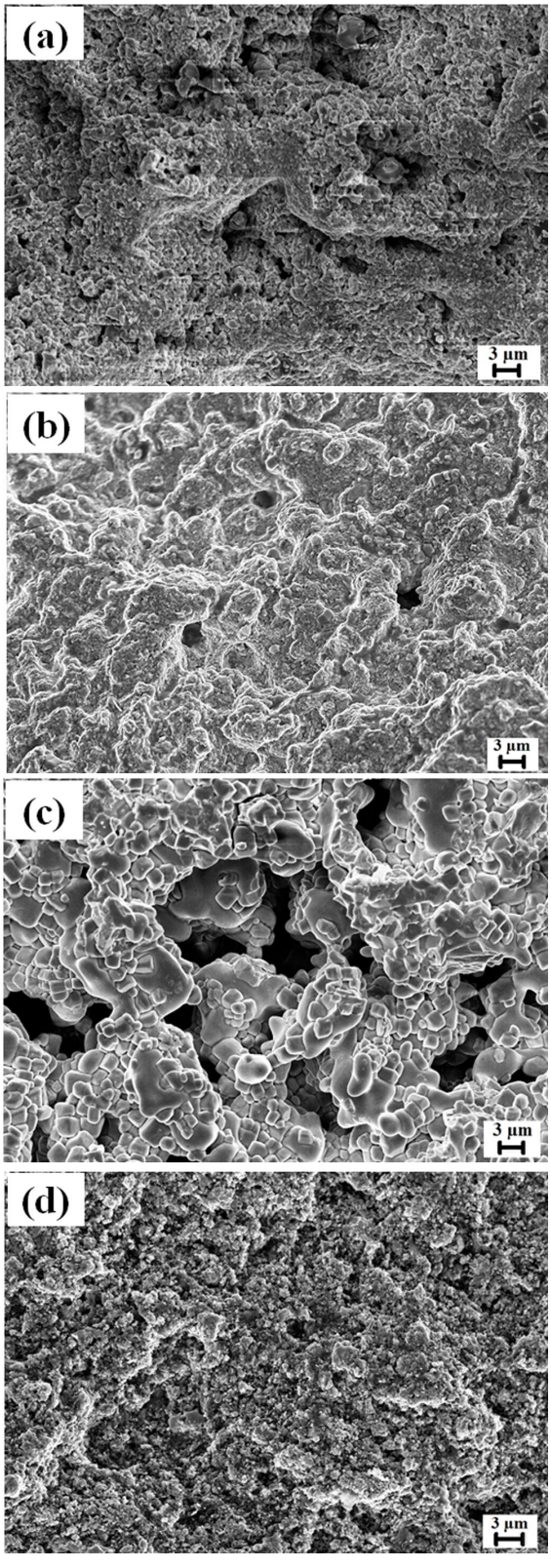

Fig. 5. FESEM images of BBFO/30PFs samples (a) BBH, (b) BBP, (c) BBU and (d) BBG.

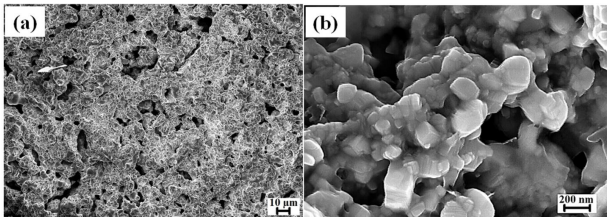

Fig. 6. FESEM micrographs (a) microstructure of BBU porous sample at low magnification showing a mean pore size of 7.5 µm (b) nano-sized grains formed on the cell walls of BBU sample.

Therefore, the grains with different morphologies were observed in some regions. Such hexagonal shapes of bismuth ferrite phase were observed earlier for $Bi_{0.8}Ba_{0.2}FeO_3$ compound [22].

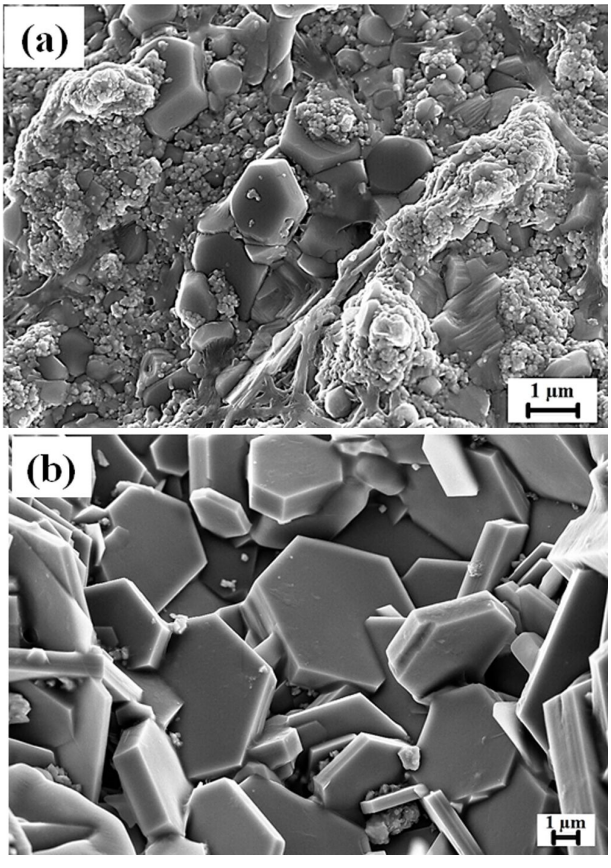

Fig. 7. FESEM micrographs of (a) BBP, (b) BBG porous samples showing some hexagonal grains.

BET measurement shows a specific surface area of 4.535 m^2/g for the BBU porous sample. The

grain size (D_{BET}) was calculated by the following equation [11]:

$$D_{BET} = \frac{6}{\rho_{Crystal} \cdot S_{BET}} \quad (2)$$

where $\rho_{Crystal}$ is the crystallographic density of $BiFeO_3$ [11] and S_{BET} is the surface area according to the BET isotherm. Therefore, the grain size was measured as 150 nm by introducing these factors in equation 2. As illustrated, the calculated grain size is in a reasonable agreement with the mean grain size of 90 nm (almost all grains are in the range of 50 to 200 nm) obtained from FESEM images (Fig. 6b). Moreover, mean crystallite sizes of 15 and 25 nm were obtained for porous BBU and compact BBC samples, respectively. These values are far lower than those of the grain sizes obtained from surface area and FESEM images. Hence, we can conclude that the particles on the cell wall of the porous sample are agglomerated.

The magnetic hysteresis loops (M-H) shown in Fig. 8 illustrate the effect of porosity on the magnetic properties of the BBC sample. Here, the reason behind the selection of BBC and BBU samples for magnetic analysis is that these samples exhibit the highest purity of $Bi_{0.8}Ba_{0.2}FeO_3$ phase which is detectable with XRD analysis. Indeed, the magnetic properties are dramatically influenced by the minor amount of impurity phases, and thus other samples were not taken into consideration. It is noteworthy that the presence of typically ferromagnetic hysteresis loops at these samples is more likely due to the destruction of the cycloidal spin structure of $BiFeO_3$, which can arise from substitution of Bi^{3+} by Ba^{2+} ions or making solid solution with other ABO_3 perovskite materials (e.g. $BiFeO_3$–$BaTiO_3$) [6, 34, 35]. The data presented in the inset of Fig. 8 confirm a decrease in saturation magnetization (M_s) from 2.31 in the compact sample to 1.85 A·m^2/kg in the porous one. It should be noted that the porous and the compact samples are not saturated even under applied magnetic field of 1200 kA/m. It is well known that saturation magnetization is a measure of the total amount of magnetic materials in a sample [16]. Naturally, magnetization per unit volume of BBC compact sample is higher than that of the BBU sample. On the other hand, the coercive field (H_c) increased from 284 to 380 kA/m with increasing porosity. The relatively high H_c value of BBU porous sample obtained in this work is higher than those reported for doped bismuth ferrites bulk [22–24] or other porous ferrites [36, 37].

As it is well known the coercive filed is intimately related to the grain size, and a large grain size (D > 15 to 20 μm) often makes a multi-domain magnetic structure. On the other hand, a single domain magnetic structure (D < 0.1 μm) is an ideal structure for large H_c [16]. Therefore, the high coercive filed of the BBU sample could be a natural evidence of the single-domain behavior of the grains in this sample. FESEM images of this sample also confirm the nano-scale grains on the pores wall (Fig. 6b).

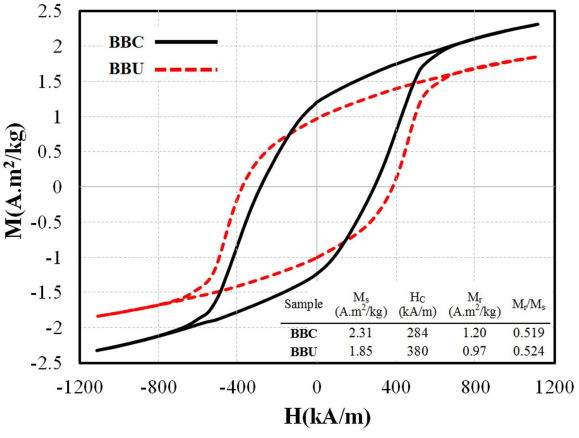

Fig. 8. Room temperature hysteresis loops (M-H) of porous BBU and compact BBC samples.

Moreover, Igarashi et al. [38] plotted the porosity dependence of demagnetizing factor, and observed that with increasing porosity, the demagnetizing factor increases linearly [39, 40]. Also, they found that uniformly small pores strongly influenced the demagnetizing factor rather than the pores with large size. Hence, another reason for such a great magnitude of H_c could be related to the uniform pore size of this porous sample with a mean pore size of 7.5 μm.

Also, porosity is an important microstructural feature limiting the movement of domain walls, and reducing the permeability [41]. Permeability

Table 2. Comparison between the RT magnetic properties of BBU porous sample with some porous structures reported earlier.

Porous sample	H_c [kA/m]	M_s [A·m^2/kg]	M_r [A·m^2/kg]	Squareness (M_r/M_s)	Reference
BBFO/30wt.% urea	380	1.85	0.97	0.524	Current work
SiOC/35wt.% PMMA	0.7	17	0.06	0.004	[16]
$BaFe_{12}O_{19}$/PU	46.4	56.5	12.1	0.214	[37]
Ni–Zn ferrite/wood	5.49	56	–	–	[36]

decreases when the grains become smaller and the porosity increases. Obviously, functional application of bismuth ferrite multiferroic requires to overcome practical obstacles such as hindering the motion of domain walls in $BiFeO_3$, which can bring about some new applications of this material [3].

The correlation between porosity and magnetic properties was investigated earlier and it was found that remanent magnetization decreases with increasing porosity [38]. In the present study, M_r decreases from 1.2 A·m^2/kg in a compact sample to 0.97 A·m^2/kg in porous sample, which is in the accordance with the above finding. Contrary to this, Topal et al. [42] reported M_r of 8.8 and 12.1 A.m^2/kg for compact and the porous samples, respectively.

Squareness factor (M_r/M_s) is almost identical for compact and porous samples. It has been reported that the high value of squareness factor ($M_r/M_s > 0.5$) indicated single-domain grains, and low value of this factor ($M_r/M_s < 0.5$) was a chracteristic of multi-domain particles [16, 37, 43]. For BBU sample, the squareness factor was calculated as 0.524 which is slightly higher than the theoretical estimation for single-domain particles. Therefore, the large coercivity of 380 kA/m and the squareness factor (M_r/M_s) higher than 0.5 were two evidences which showed the existence of single domain particles in the urea-derived porous bismuth ferrite ceramics. Table 2 presents the obtained magnetic results in this study which are compared with the earlier results of magnetic ferrites.

4. Conclusions

Single-phase bismuth ferrite porous ceramics was successfully fabricated by sacrificial pore former method utilizing Ba-doped $BiFeO_3$ as the starting powder and urea as the pore forming agent. XRD analysis showed that Ba-dopant enhances the stability of bismuth ferrite phase in the final porous ceramics. Urea-derived porous $Bi_{0.8}Ba_{0.2}FeO_3$ exhibits the best multifunctional properties. Well defined nanostructured cell walls with a mean grains size of 90 nm were observed in the above sample which is in accordance with the particle size calculated from S_{BET}. Magnetic properties results revealed that by increasing porosity, remanent (M_r) and saturation (M_S) magnetization decreased, and also coercivity (H_C) increased. Moreover, the large coercivity of 380 kA/m and the squareness factor (M_r/M_s) higher than 0.5 were two evidences which showed single domain particles in the urea-derived porous bismuth ferrite ceramics.

Acknowledgements

The financial supports of this work by the University of Tehran and Iran Nanotechnology Initiative Council are gratefully acknowledged.

References

[1] DAVIS M.E., *Nature*, 417 (2002), 813.
[2] EERENSTEIN W., MATHUR N., SCOTT J., *Nature*, 442 (2006), 759.
[3] BÉA H., PARUCH P., *Nat. Mater.*, 8 (2009), 168.
[4] SCOTT J., *Nat. Mater.*, 6 (2007), 256.
[5] GREEN D.J., COLOMBO P., *MRS. Bull.*, 28 (2003), 296.
[6] CATALAN G., SCOTT J.F., *Adv. Mater.*, 21 (2009), 2463.
[7] VALANT M., AXELSSON A.-K., ALFORD N., *Chem. Mater.*, 19 (2007), 5431.
[8] SELBACH S.M., EINARSRUD M.-A., GRANDE T., *Chem. Mater.*, 21 (2008), 169.
[9] MOSTAFAVI E., ATAIE A., AHMADZADEH M., *Adv. Mater. Res.*, 829 (2014), 683.
[10] KHOMCHENKO V., SHVARTSMAN V., BORISOV P., KLEEMANN W., KISELEV D., BDIKIN I., *Acta. Mater.*, 57 (2009), 5137.
[11] SELBACH S.M., EINARSRUD M.A., TYBELL T., GRANDE T., *J. Am. Ceram. Soc.*, 90 (2007), 3430.

[12] PULLAR R.C., *Prog. Mater. Sci.*, 57 (2012), 1191.
[13] ZHANG L., MAO Z., THOMASON J.D., WANG S., HUANG K., *J. Am. Ceram. Soc.*, 95 (2012), 1832.
[14] STUDART A.R., GONZENBACH U.T., TERVOORT E., GAUCKLER L.J., *J. Am. Ceram. Soc.*, 89 (2006), 1771.
[15] SARIKAYA A., DOGAN F., *Ceram. Int.*, 39 (2013), 403.
[16] BIASETTO L., FRANCIS A., PALADE P., PRINCIPI G., COLOMBO P., *J. Mater. Sci.*, 43 (2008), 4119.
[17] XIAO W., MIAO C., YIN X., ZHENG Y., TIAN M., LI H., *J. Power. Sources*, 252 (2014), 14.
[18] HONG-TAO S., MING-TANG W., PING L., XI Y., *Sens. Actuat.*, 19 (1989), 61.
[19] PARK T.-J., PAPAEFTHYMIOU G.C., VIESCAS A.J., MOODENBAUGH A.R., WONG S.S., *Nano. Lett.*, 7 (2007), 766.
[20] YU X.L., WANG Y., HU Y.M., CAO C.B., CHAN H.L.W., *J. Am. Ceram. Soc.*, 92 (2009), 3105.
[21] MOSTAFAVI E., ATAIE A., AHMADZADEH M., PALIZDAR M., COMYN T.P., BELL A.J., *Mater. Chem. Phys.*, 162 (2015), 106.
[22] CHAUDHURI A., MANDAL K., *J. Magn. Magn. Mater.*, 353 (2014), 57.
[23] DAS R., MANDAL K., *J. Magn. Magn. Mater.*, 324 (2012), 1913.
[24] GAUTAM A., RANGRA V., *Cryst. Res. Technol.*, 45 (2010), 953.
[25] MOSTAFAVI E., ATAIE A., *J. Mater. Sci. Technol.*, 31 (2015), 798.
[26] CULLITY B.D., STOCK S.R., *Elements of X-ray Diffraction*, 3rd ed, Prentice hall Upper Saddle River; New Jersey, 2001.
[27] CARVALHO T., TAVARES P., *Mater. Lett.*, 62 (2008), 3984.
[28] SHANNON R.T., *Acta. Crystallogr. A*, 32 (1976), 751.
[29] MAKHDOOM A., AKHTAR M., RAFIQ M., HASSAN M., *Ceram. Int.*, 38 (2012), 3829.
[30] PARK K., *Mater. Sci. Eng. B*, 107 (2004), 19.
[31] ZHANG H., LI J.-F., ZHANG B.-P., *Acta. Mater.*, 55 (2007), 171.
[32] ZHOU Z., CHEN J., *Sens. Actuat. B-Chem.*, 13 (1993), 132.
[33] JOHNSSON M., LEMMENS P., *Crystallography and chemistry of perovskites*, in: KRONMULLER H., PARKIN S. (Eds), *Handbook of Magnetism and Advanced Magnetic Materials*, Willey-VCH Verlag GmbH & Co. KGaA, Berlin, 2007.
[34] KOWAL K., KOWALCZYK M., CZEKAJ D., JARTYCH E., *Nukleonika*, 60 (2015), 81.
[35] WANG D., GOH W., NING M., ONG C., *Appl. Phys. Lett.*, 88 (2006), 212907.
[36] SIA C.K., SASAKI Y., ADACHI N., OTA T., *J. Ceram. Soc. Jpn.*, 117 (2009), 958.
[37] TOPAL U., BAKAN H.I., *Mater. Chem. Phys.*, 123 (2010), 121.
[38] IGARASHI H., OKAZAKI K., *J. Am. Ceram. Soc.*, 60 (1977), 51.
[39] CULLITY B.D., GRAHAM C.D., *Introduction to magnetic materials*, John Wiley & Sons, 2011.
[40] RIKUKAWA H., *IEEE Trans. Magn.*, 18 (1982), 1535.
[41] GOLDMAN A., Modern ferrite technology: Springer, 2006.
[42] TOPAL U., BAKAN H.I., *J. Eur. Ceram. Soc.*, 30 (2010), 3167.
[43] WALKER M., MAYO P., O'GRADY K., CHARLES S., CHANTRELL R., *J. Phys. Condens. Matter.*, 5 (1993), 2793.

Received 2015-08-04
Accepted 2015-11-26